A conceptual model of light coupling by pillar diffraction gratings

K. R. Catchpole[a)]
School of Photovoltaic and Renewable Energy Engineering, University of New South Wales, Sydney, New South Wales 2052, Australia

M. A. Green
Centre of Excellence for Advanced Silicon Photovoltaics, University of New South Wales, Sydney, New South Wales 2052, Australia

Diffractive structures such as pillar gratings are a promising way of coupling light into or out of thin semiconductor devices, for applications in thin film solar cells and light-emitting diodes. In this paper we show that the diffuse transmittance behavior of pillar gratings can be understood using the concept of grating mode interference and that the optimum heights of the grating and an estimate of the optimum period can be predicted with the effective index method. Furthermore, the method also gives good results for structures outside the range for which it was derived, including circular pillars and quasiperiodic structures. We also show that pillar gratings offer substantially improved performance over groove gratings for thin film silicon solar cells. © *2007 American Institute of Physics*. [DOI: 10.1063/1.2710765]

I. INTRODUCTION

Because silicon is an indirect band gap semiconductor, light trapping is important for increasing the absorptance of silicon solar cells. With the trend to decrease the thickness of solar cells to reduce material costs, light trapping is becoming even more crucial for good device performance. For wafer-based cells, conventional light-trapping structures such as inverted or random pyramids, which are about 5 μm in height, can be used. However, for thin film devices which may be only a few microns thick, such structures are not suitable. Diffractive structures such as gratings formed from grooves or pillars provide an attractive alternative, as they are only a few hundred nanometers in height.[1] It has been shown that groove-type gratings can lead to a significant increase in absorptance.[1,2] Furthermore, diffractive structures can also be used to dramatically enhance the light extraction from light-emitting diodes. Windisch *et al.* achieved an external quantum efficiency of 40% from thin film GaAs light-emitting diodes using a quasiperiodic pillar-type diffractive structure formed by nanosphere lithography.[3]

The performance of groove gratings depends on the polarization of the incident wave, resulting in optimum grating parameters that are a compromise between the optimum parameters for the two types of incident polarization. We might expect that pillar-type diffraction gratings provide better light trapping and light extraction than groove gratings, because the dependence on the polarization of the incident wave is removed. Previously we have applied simplified modal analysis, developed by Tishchenko[4] and Clausnitzer *et al.*,[5] to provide a conceptual model of diffuse transmittance by rectangular groove gratings for light-trapping applications.[6] In this paper we show that simplified modal analysis can also be applied to pillar-type diffraction gratings by using the effective index method[7,8] to calculate approximately the effective indices of the grating modes. We find excellent agreement with rigorous numerical results. Thus the physically intuitive model of interference of grating modes is extended to pillar-type structures. This allows the optimum heights of the structures to be calculated, and the optimum periods roughly predicted, without the need for extensive numerical calculations. We also show that pillar gratings have the potential to produce significantly higher short-circuit current in thin film silicon solar cells than groove gratings.

II. THEORY

In this section we summarize simplified modal analysis and describe how the effective index method can be applied to pillar-type grating structures.

A. Simplified modal analysis

It has been shown that the origin of the optimum values of height and period for rectangular groove gratings can be understood with the help of simplified modal analysis.[4–6] When light is incident on a diffraction grating, it is diffracted into a number of different orders or modes. Simplified modal analysis is based on the fact that as well as the diffracted modes propagating outside the grating, there are electromagnetic modes that propagate inside the grating. The diffraction process can then be thought of as a coupling between the incident light, the grating modes, and the diffracted modes. The grating modes have different effective refractive indices and thus accumulate a phase difference as they propagate through the grating. This results in an approximately periodic dependence of the diffraction efficiencies on grating height. The optimal values of grating height h occur when there is a phase difference between the grating modes of π, 3π, 5π, etc. For the zeroth and second grating modes, for example, this leads to optimal values of h at odd integral multiples of

a)Electronic mail: k.catchpole@unsw.edu.au

101, 063105-1

$$h_{\text{opt}} = \frac{\lambda}{2|n_2^{\text{eff}} - n_0^{\text{eff}}|},\tag{1}$$

where n_2^{eff} and n_0^{eff} are the effective refractive indices of the second and zeroth grating modes, respectively. (The first grating mode does not take part because it has a field distribution that is an odd function with respect to the vertical axis of symmetry of the grating, which means that it does not couple to normally incident light.) For rectangular groove gratings the values of n^{eff} are solutions of the characteristic grating equation:

$$f(n^{\text{eff}}) = \cos(k_{xr}L_r)\cos(k_{xg}L_g) - \frac{1}{2}\left(\tau\frac{k_{xr}}{k_{xg}}\right.$$
$$\left. + \frac{1}{\tau}\frac{k_{xg}}{k_{xr}}\right)\sin(k_{xr}L_r)\sin(k_{xg}L_g) = \cos(k_{x0}L),\tag{2}$$

where $k_{x0} = k_0 \sin(\theta_{\text{in}}) = (2\pi/\lambda)n_a \sin(\theta_{\text{in}})$ is the x component of the wave vector of the incident wave, and

$$k_{xi} = k_0[n_i^2 - (n^{\text{eff}})^2]^{1/2}, \quad i = r, g\tag{3}$$

are the x components of the wave vectors in the ridges and grooves of the grating, respectively. L_r is the width of the ridges and L_g is the width of the grooves, with the period $L = L_r + L_g$. τ is equal to 1 for TE polarization (i.e., where there is only one component of the electric field, and it is perpendicular to the direction of propagation), and τ is equal to n_r^2/n_g^2 for TM polarization (where there is only one component of the magnetic field, perpendicular to the direction of propagation). n_r and n_g are the refractive indices of the ridge and grooves. n_a is the refractive index of the incident medium, and in most cases will be equal to n_g. Equation (2) is also known as the photonic crystal equation,[9] since the problem of finding the grating modes of a one-dimensional (1D) lamellar grating is the same as finding the modes of a 1D photonic crystal. Thus for the 1D case of rectangular grooves the effective refractive indices can be easily determined. We may anticipate that for the two-dimensional (2D) case of pillars there also exist grating modes that can be characterized by effective refractive indices. For the 2D case there does not exist an expression corresponding to Eq. (2). However, we show in the next section that the effective index method can be used to obtain good approximations for the effective refractive indices.

The concept of interference of grating modes has also been applied to photonic crystal films, in which the period is sufficiently short that only the zeroth diffracted order propagates in reflectance or transmittance, but more than one grating mode may propagate inside the film. The broadband background reflectance and narrow resonances observed in these films have both been successfully explained using grating mode interference.[10–12] For the case where only one mode propagates in all regions, simplified modal analysis reduces to effective medium theory and predicts peaks and dips in the reflectance due to interference of the zeroth grating mode with itself, similar to the interference seen in a thin film.[4]
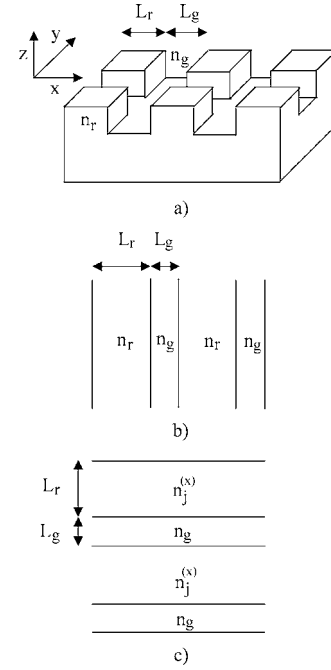

FIG. 1. (a) The pillar diffraction grating modeled. (b) Plan view of the 1D grating structure with the same parameters as the pillar structure in the x direction. (c) Plan view of the equivalent grating structure used for the y direction. Here the values of $n_j^{(x)}$ are the effective index values calculated for the structure used for the x direction.

B. The effective index method for square pillar gratings

The effective index method (EIM) involves calculating the modes for two separate one-dimensional problems. It is based on approximating the structure to be modeled by a structure in which the variations in the x and y directions are not coupled, and then applying separation of variables. The method was demonstrated by Knox and Toulios for rectangular waveguides[13] and has since been applied to a wide range of systems including a variety of waveguide shapes and coupled waveguides.[8,14] Very recently the model has also been applied to 2D gratings in the case where only one waveguide mode (the zeroth order) propagates, i.e., the subwavelength limit.[15] In this paper we show that the EIM can also be applied to 2D grating structures with several propagating modes and that in combination with simplified modal analysis it gives good predictions of the optimum height for high diffuse transmittance for these structures, as well as approximate estimates of the optimum period.

The parameters of the 2D grating are shown in Fig. 1(a). Because of the geometry of the grating structure, the z dependence of the field can be separated from the (x, y) dependence, e.g., for the electric field,

$$E(x, y, z) = u(x, y)v(z),\tag{4}$$

where the time dependence $e^{i\omega t}$ has been omitted. $v(z)$ has the form $v(z) = A \exp(-ik_0 n_{ij} z) + B \exp(+ik_0 n_{ij} z)$ and describes propagating or evanescent transmitted and reflected waves with effective refractive index n_{ij}. After separation of the z dependence, the full vector wave equation obtained from Maxwell's equations can be further decoupled into the reduced vector wave equations:[16]

$$\nabla_t^2 E_x + [n^2 k_0^2 - n_{\text{eff}}^{(x)} k_0^2] E_x + \frac{\partial}{dx}\left(\frac{E_x}{n^2}\frac{\partial n^2}{\partial x}\right) = 0, \tag{5}$$

$$\nabla_t^2 E_y + [n^2 k_0^2 - n_{\text{eff}}^{(y)} k_0^2] E_y + \frac{\partial}{dy}\left(\frac{E_y}{n^2}\frac{\partial n^2}{\partial y}\right) = 0, \tag{6}$$

where E_x and E_y are the x and y components of the electric field, $\nabla_t = (\partial/\partial x\ \mathbf{x} + \partial/\partial y\ \mathbf{y})$, and $n^2(x,y)$ is the dielectric function profile. The effective indices calculated from the two equations are in general different. The solutions represent two types of modes, sometimes called quasi-TE and quasi-TM, or $E^{(x)}$ and $E^{(y)}$ modes. The decoupling of the full vector wave equation into the reduced vector wave equations is exact for slab waveguides[14] and for 1D gratings. It is also an accurate approximation in a number of cases, including for rectangular waveguides far from cutoff,[14] because the guided modes of rectangular waveguides are approximately linearly polarized far from cutoff.[17] However, we find from our comparison of the results of the EIM with those of rigorous coupled wave analysis[18–20] (RCWA) that the EIM also provides a good estimate of the effective indices of the grating modes for the cases considered here even close to cutoff.

The procedure for determining the effective index $n_{ij}^{(x)}$ of the $E_{ij}^{(x)}$ mode via the x-method version of the EIM is as follows. The first step is to determine the effective index of the jth mode, $n_j^{(x)}$, of the 1D grating structure that has the same parameters in the x direction, as shown in Fig. 1(b), for TE propagation. The second step is to determine the effective index of the ith mode for a 1D grating structure in the y direction where the refractive index of the groove region is the same as that in the original grating, but the refractive index of the high index ridge region is given by the $n_j^{(x)}$ value previously calculated [see Fig. 1(c)]. This calculation is made for TM propagation.

The y-method EIM is very similar to the x method. For the $E_{ij}^{(y)}$ mode it involves calculating the n_i values for the nth mode of a 1D grating for the TE case, and then using these as the high index values to calculate the jth mode of a 1D grating for the TM case. For further details of the y method see Ref. 7. In this paper the x method was used to calculate $E_{ij}^{(x)}$ and the y method to calculate $E_{ij}^{(y)}$ because this gives the most accurate results, according to the error expressions in Table 1 of Ref. 7, and also because it was found that they fit the results calculated with RCWA much better than the alternative of using the x method to calculate $E_{ij}^{(y)}$ and the y method to calculate $E_{ij}^{(x)}$. [The dual EIM (Ref. 7) was also tested but was found to give unphysical results.]

We can see from the description of the x-method and y-method EIMs that for a square grating $n_{ij}^{(x)} = n_{ij}^{(y)}$ Incident light that is polarized in the x direction will excite, for example, the $n_{02}^{(x)}$ and $n_{20}^{(x)}$ modes, which are the same as the $n_{20}^{(y)}$ and $n_{20}^{(y)}$ modes. Thus incident light that is polarized in the y direction will excite the same modes. The overall result is polarization independent, as we would expect. Note also that the convention used here for naming the modes is different from that normally used in the EIM in order to be consistent

n_r^2	$n_g^2 + n_r^2$ $- (n_j^{(x)})^2$
$n_g^2 + n_r^2 - (n_j^{(x)})^2$	$2n_g^2$ $- (n_j^{(x)})^2$

FIG. 2. Plan view of the unit cell of the grating structure that the x-method version of the effective index method actually solves.

with previous work on simplified modal analysis; the effective refractive index for the fundamental mode is referred to here as n_{00} rather than n_{11}.

The justification for the use of the procedure used in the EIM can be understood by examining the mathematical basis of the method. When we apply the EIM to a structure we are assuming that the dielectric function profile of interest can be approximated by a separable profile[7,21] i.e.,

$$n^2(x,y) \cong n_{\text{app}}^2(x,y) = n_{\text{app},x}^2(x) + n_{\text{app},y}^2(y). \tag{7}$$

The separable dielectric function profile leads to a separable solution for the field distribution of the mode

$$u_{ij}(x,y) = X_i(x) Y_j(y). \tag{8}$$

For the $E_{ij}^{(x)}$ mode with the x method, $E_{ij}^{(x)} = u_{ij}$, and $X_i(x)$ and $Y_j(y)$ satisfy the reduced vector wave equations

$$\frac{d^2 Y_j}{dy^2} + k_0^2[n_{\text{app},y}^2(y) - (n_j^{(x)})^2]Y_j = 0, \tag{9}$$

$$\frac{d^2 X_i}{dx^2} + \frac{d}{dx}\left(\frac{X_i}{\{n_{\text{app},x}^2 + [n_j^{(x)}]^2\}}\frac{d\{n_{\text{app},x}^2 + [n_j^{(x)}]^2\}}{dx}\right) + k_0^2\{n_{\text{app},y}^2(y) + [n_j^{(x)}]^2 - [n_{ij}^{(x)}]^2\}X_i = 0, \tag{10}$$

with

$$n_{\text{app},y}^2 = \begin{cases} n_r^2, & |y - pL| \leqslant |f_y L/2| \\ n_g^2, & |y - pL| > |f_y L/2| \end{cases} \quad \text{where } p = 0,1,2\ldots \tag{11}$$

and

$$n_{\text{app},x}^2(x) + [n_j^{(x)}]^2 = \begin{cases} [n_j^{(x)}]^2 & |x - pL| \leqslant |f_y L/2| \\ n_g^2 & |x - pL| > |f_y L/2|, \end{cases} \tag{12}$$

where $f_y = L_r/(L_r + L_g)$. Equations (9) and (10) are the equations for the TE solution of the structure shown in Fig. 1(b) and the TM solution of the structure shown in Fig. 1(c), respectively. In Eqs. (11) and (12) we have expressed the separable dielectric function profile in terms of the refractive indices of the original structure and the effective indices of the grating modes $n_j^{(x)}$. The resulting profile is shown in Fig. 2.

The approximate form of the refractive index distribution shown in Fig. 2 has a higher value than the original structure in the regions directly adjacent to the central high

index region and a lower value in the corners. The approximate refractive index distribution produces good agreement with exact models for modes where most of the power is transferred within the central high index region, i.e., where the modes are far from cutoff, because the separable and nonseparable profiles are identical in the high index region and differ only in the low index surrounding regions.[22] We show here that the EIM provides a sufficiently good approximation even near mode cutoffs to allow effective indices and optimum heights (as well as estimates of optimum periods) for maximum diffuse transmittance to be calculated for semiconductor gratings.

The power transfer between the incident light and diffracted orders in simplified modal analysis is determined by the modal overlap and impedance matching of the modes involved. Impedance matching occurs when the two modes involved have the same effective refractive indices. The overlap integral of two modes is given by

$$\langle E^{\text{in}}(x,y), u_{ij}(x,y) \rangle = \frac{|\int E^{\text{in}}(x,y)u_{ij}(x,y)dxdy|^2}{\int |E^{\text{in}}(x,y)|^2 dxdy \int |u_{ij}(x,y)|^2 dxdy}. \quad (13)$$

An overlap integral is a measure of the similarity of two electromagnetic field modes. Two completely dissimilar (i.e., orthogonal) modes will not interfere, i.e., there will be no power transfer. For more details on how impedance matching and overlap integrals determine the diffraction efficiency into a particular mode, see Appendix A of Ref. 4; here we simply use the overlap integrals to estimate the relative importance of the coupling of different modes.

III. RESULTS AND DISCUSSION

In this section the results of simplified modal analysis using the EIM are compared with numerical results calculated with RCWA. RCWA allows the diffracted power into each mode to be accurately calculated for arbitrary grating structures, but does not provide any physical insight into the reasons for the behavior of the grating, and is computationally intensive for pillar structures. We focus our discussion on the practically interesting cases of silicon pillars on silicon for light incident from glass and from air, TiO_2 pillars on silicon, and AlGaAs pillars on GaAs.

A. Silicon pillars on silicon

Figure 3(a) shows the results calculated with RCWA for the diffuse transmittance (i.e., the total transmittance into all diffracted orders except the zeroth order) for the case of silicon pillars on an infinite silicon substrate, with light normally incident from glass. Also plotted are the results of a calculation using Eq. (1) and the EIM for the heights of maximum diffuse transmittance. We can see that there is very good agreement between the two calculations, particularly for the first peak which is of most interest in practical devices. The broad peaks in optimum heights seen in the RCWA results are due to the fact that there are two n_{02}
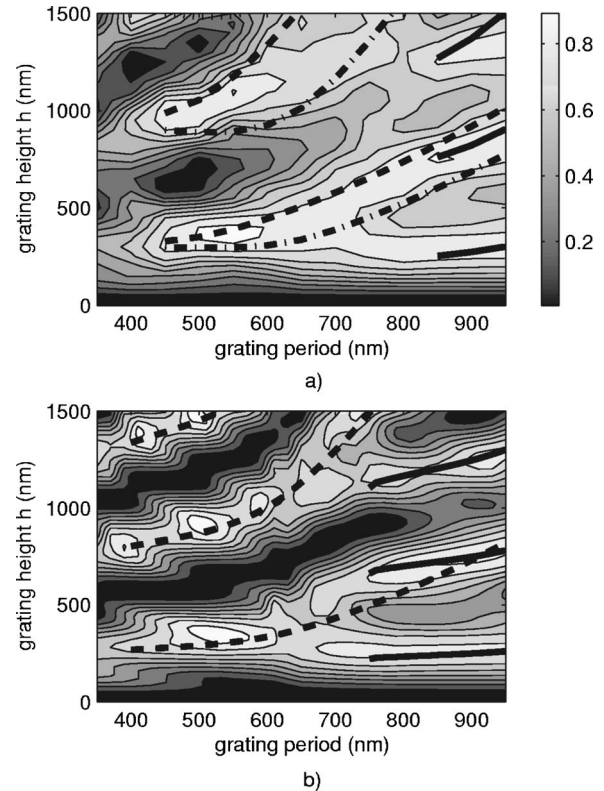

FIG. 3. (a) Diffuse transmittance for silicon pillars on an infinite silicon substrate with light of wavelength 950 nm normally incident from glass ($n=1.5$), calculated with RCWA (contours), along with the heights of maximum diffuse transmittance calculated using the EIM. The fractional area of the pillars is $f=(f_x)^2=0.5$ (where $f_x=L_r/L=0.707$). The peaks in diffuse transmittance are due to interference between the n_{00} and $n_{02}^{(x)}$ modes (dashed lines), n_{00} and $n_{02}^{(y)}$ modes (dash-dot lines), and n_{00} and $n_{04}^{(x)}$ modes (solid lines). (b) The corresponding plots for a rectangular silicon grating under TM illumination with $f_x=0.707$. Peaks in diffuse transmittance are due to interference between the n_0 and n_2 modes (dashed lines) and n_0 and n_4 modes (solid lines).

modes, $n_{02}^{(x)}$ and $n_{02}^{(y)}$, with slightly different effective indices, both of which interfere with the n_{00} mode to produce peaks in the diffuse transmittance. Note that since the pillars of the grating are square, there is only one n_{00} mode [$n_{00}^{(x)}=n_{00}^{(y)}$]. As the grating period increases, additional grating modes can propagate, and above $L=850$ nm the $n_{04}^{(x)}$ mode leads to extra peaks in the diffuse transmittance. [The onset of $n_{04}^{(y)}$ is beyond $L=950$ nm.] The diffuse transmittance for an equivalent groove grating under TM illumination is shown in Fig. 3(b) for comparison.

The diffuse transmittance results for pillars are similar to those calculated for rectangular groove gratings for the TM case, but shifted slightly to higher periods and heights, as can be seen from a comparison of Figs. 3(a) and 3(b). This is because the effect of the TE calculation in the EIM is to reduce the effective refractive indices involved in the following TM calculation. For example, in calculating $n_{20}^{(x)}$, we first calculate n_0^{eff} for a single grating, for TE incidence. The value of n_0^{eff} is always somewhat smaller than n_r. (For a rectangular grating with period 550 nm, with $n_r=3.6$, and light of wavelength 950 nm incident from glass, $n_0^{\text{eff}}=3.4$.) The next step in calculating $n_{20}^{(x)}$ is to calculate n_2^{eff} for TM incidence for a grating with $n_j^{(x)}=n_0^{\text{eff}}$ for the high index region. Thus the
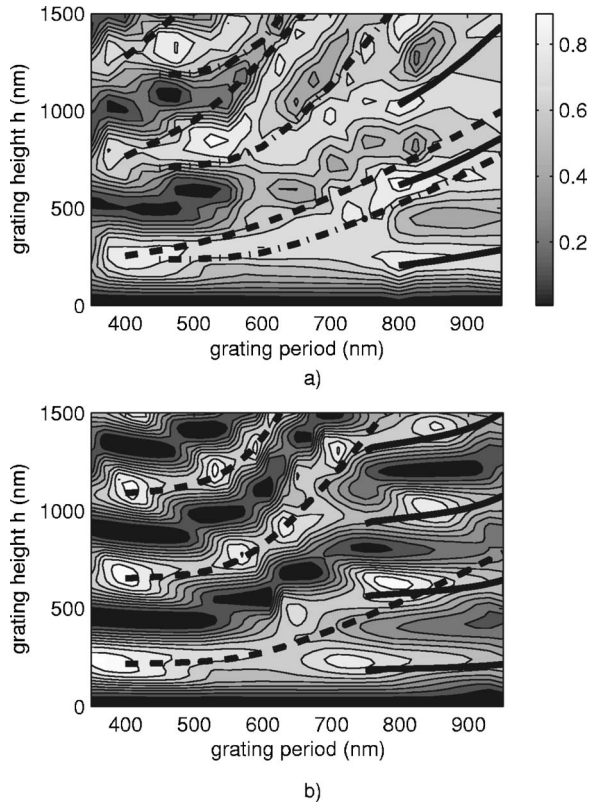
FIG. 4. (a) Diffuse transmittance for silicon pillars on an infinite silicon substrate with $f=0.5$ ($f_x=0.707$) and light of wavelength 950 nm normally incident from air calculated with RCWA (contours), along with the heights of maximum diffuse transmittance calculated using the EIM. Peaks in diffuse transmittance are due to interference between the n_{00} and $n_{02}^{(x)}$ modes (dashed lines), n_{00} and $n_{02}^{(y)}$ modes (dash-dot lines), and n_{00} and $n_{04}^{(x)}$ modes (solid lines). The onset of $n_{04}^{(y)}$ is beyond $L=950$ nm. (b) The corresponding plots for a rectangular silicon grating on an infinite silicon substrate with $f_x=0.707$. Peaks in diffuse transmittance are due to interference between the n_0 and n_2 modes (dashed lines) and n_0 and n_4 modes (solid lines).

results for a pillar grating are similar to the TM results for a 1D grating with somewhat smaller refractive index. The peaks are broader in 2D because there are both $E_{ij}^{(x)}$ and $E_{ij}^{(y)}$ modes involved in the interference, with slightly different effective indices when i does not equal j.

Figure 4(a) shows the results for silicon pillars on an infinite silicon substrate with light normally incident from air. Again we can see good agreement between the RCWA results and the results of the EIM. In this case we can see more clearly from the RCWA results the fact both the $n_{02}^{(x)}$ and $n_{02}^{(y)}$ modes interfere with the n_{00} mode. We see separate narrow peaks, rather than a broad peak, in the period range of 600–700 nm at heights of 750–1500 nm. In this case, the plots for the pillars and the rectangular grating look different for large grating heights, because in this range the values of $n_{02}^{(x)}$ and $n_{02}^{(y)}$ are sufficiently different to lead to separate peaks. However, for small grating heights, the plots are still similar [Figs. 4(a) and 4(b)].

The n_{22} mode does not play a significant part in determining the diffuse transmittance. We can understand this by calculating the overlap integrals between the incident mode and the various grating modes. Using the separable approxi-

TABLE I. Overlap integrals for pillar gratings and equivalent 1D gratings used in the EIM, for the case where $L=600$ nm for silicon pillars with light incident from air, $\lambda=950$ nm, and $f=0.5$ ($f_x=0.707$).

Overlaps for 1D equivalent gratings		Total overlaps for 2D gratings	
$\langle E^{\text{in}}, X_0 \rangle$	0.742	$\langle E^{\text{in}}, E_{00}^{(x)} \rangle$	0.442
$\langle E^{\text{in}}, Y_0 \rangle$	0.596	$\langle E^{\text{in}}, E_{20}^{(x)} \rangle$	0.091
$\langle E^{\text{in}}, X_2 \rangle$	0.148	$\langle E^{\text{in}}, E_{02}^{(x)} \rangle$	0.088
$\langle E^{\text{in}}, Y_2 \rangle$	0.122	$\langle E^{\text{in}}, E_{22}^{(x)} \rangle$	0.018

mations of the field distributions as calculated with the EIM, for normal incidence with the x method the overlap integrals can be written as

$$\langle E^{\text{in}}(x,y), u_{ij}(x,y) \rangle = \frac{\left| \int E^{\text{in}}(x,y) u_{ij}(x,y) dx dy \right|^2}{\int |E^{\text{in}}(x,y)|^2 dx dy \int |u_{ij}(x,y)|^2 dx dy}$$

$$= \frac{\left| \int X_j(x) dx \right|^2 \left| \int Y_i(y) dy \right|^2}{\int |X_j(x)|^2 dx \int |Y_i(y)|^2 dy}$$

$$= \langle E^{\text{in}}(x,y), X_j(x) \rangle \langle E^{\text{in}}(x,y), Y_i(y) \rangle.$$

(14)

That is, to calculate the overlap integrals for the pillar grating, we only need to calculate the overlap integrals for the 1D equivalent gratings used in the EIM and multiply them together. From Eq. (14) we can see directly that since for 1D gratings the overlap between incident mode and the zeroth grating mode $\langle E^{\text{in}}, E_0 \rangle$ tends to be larger than the overlap with the second grating mode $\langle E^{\text{in}}, E_2 \rangle$, the overlap $\langle E^{\text{in}}, E_{02}^{(x)} \rangle = \langle E^{\text{in}}, X_2 \rangle \langle E^{\text{in}}, Y_0 \rangle$ for the pillar grating will be larger than the overlap $\langle E^{\text{in}}, E_{22}^{(x)} \rangle = \langle E^{\text{in}}, X_2 \rangle \langle E^{\text{in}}, Y_2 \rangle$. An example of the values of these overlap integrals, for the case where $L=600$ nm for silicon pillars with light incident from air, $\lambda=950$ nm, and $f=0.5$ ($f_x=0.707$), is given in Table I. We can see that the overlap with the $E_{22}^{(x)}$ mode is very small compared with the overlaps with the $E_{20}^{(x)}$ and $E_{02}^{(x)}$ modes.

In order to estimate the potential benefit of using pillar-type structures rather than groove-type structures, we calculate the potential short-circuit current for thin film silicon solar cells with Si/air front surface gratings of groove type and pillar type, each with the optimum parameters for maximum diffuse transmittance. The rear of each cell is a flat Ag reflector and the effective thickness of silicon in each case is 3 μm. (The effective thickness is used in order to take account of absorption in the grating region and is the thickness of an equivalent volume of planar silicon.) The optimum parameters are $L=650$ nm and $h=300$ nm for the groove structure and $L=450$ nm and $h=250$ nm for the pillar structure. We have shown previously[6] that for cells with front surface rectangular groove gratings and flat rear reflectors the potential J_{sc} is correlated with the diffuse transmittance and that the parameters for maximum diffuse transmittance are the same as the parameters for maximum J_{sc}. Although we
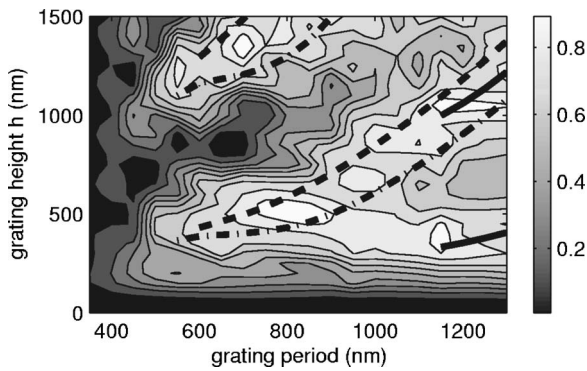
FIG. 5. Diffuse transmittance for TiO$_2$ pillars ($n=2.6$) on an infinite silicon substrate (for light of wavelength 950 nm normally incident from air), with $f=0.5$ ($f_x=0.707$) calculated with RCWA (contours), and the heights of maximum diffuse transmittance calculated using the EIM. Peaks in diffuse transmittance are due to interference between the n_{00} and $n_{02}^{(x)}$ modes (dashed lines), n_{00} and $n_{02}^{(y)}$ modes (dash-dot lines), and n_{00} and $n_{04}^{(x)}$ modes (solid lines). The onset of $n_{04}^{(y)}$ is beyond $L=1300$ nm.
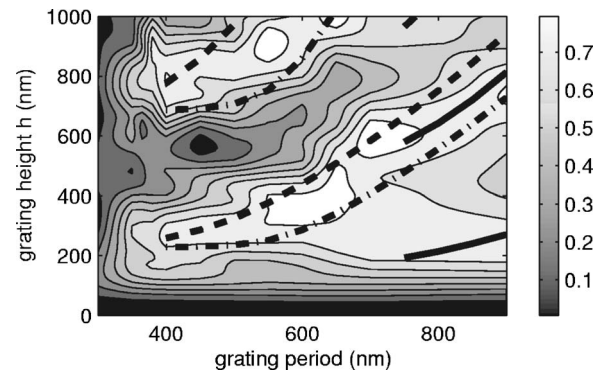

FIG. 6. Diffuse transmittance for circular pillars of AlGaAs on an infinite GaAs substrate with $f=0.5$ as a function of grating period and height for a wavelength of 870 nm, calculated with RCWA (contours). The period range $L=300–900$ nm corresponds to a pillar diameter range of 240–720 nm for the circular pillars. The EIM results (lines) are calculated for a square pillar grating with the same values of L and f. Peaks in diffuse transmittance are due to interference between the n_{00} and $n_{02}^{(x)}$ modes (dashed lines), n_{00} and $n_{02}^{(y)}$ modes (dash-dot lines), and n_{00} and $n_{04}^{(x)}$ modes (solid lines).

do not investigate it here, we would expect this to also be the case for pillar diffraction gratings, because as for the case of groove gratings, at the optimum value of period all the diffusely transmitted light in the wavelength range for light trapping is outside the escape cone. The potential J_{sc} for the cell with a pillar-type grating is 23.2 mA/cm^2, compared with 20.7 mA/cm^2 for the cell with the groove grating, showing that pillar gratings offer substantially improved performance. It should also be possible to fabricate pillar gratings without much increase in process complexity compared to the processes required for groove gratings and possibly even with simpler processes. Using interference lithography, pillar gratings only require one extra exposure. Furthermore, nanosphere lithography may be simpler and more practical than interference lithography and naturally forms pillar-type structures.

B. TiO$_2$ pillars on silicon

Simplified modal analysis and the EIM can be applied to a range of different material systems of interest. As an example, Fig. 5 shows the results for TiO$_2$ pillars on an infinite silicon substrate. For this case the predictions of the EIM also fit very well with the results of RCWA. The same modes take part as in the cases of silicon pillars, but at larger grating periods due to the lower refractive index of TiO$_2$. Thus we can see that for a variety of cases, we can predict the optimum heights for maximum diffuse transmittance for pillar gratings on semiconductors for solar cell or light-emitting diode applications using very simple calculations made with the effective index method.

As well as the optimum heights for maximum diffuse transmittance, we can also estimate the optimum periods. We can see from the results shown on the figures that the optimum periods occur either at the onset of new grating modes where n_{20} and $n_{02} \cong n_g$ (as for Si pillars in air), or for periods 100 nm higher (e.g., Si pillars on glass), or 200 nm higher (TiO$_2$ pillars on Si in air). As the period increases beyond the onset of a new grating mode, the value of n^{eff} for that mode increases, improving the impedance match between that

mode and the transmitted diffracted orders. However, the overlap integral between the grating mode and the incident mode decreases as the period increases, and soon after n^{eff} reaches n_g, the modal overlap becomes the dominant factor in determining the optimum period.

We can also see from Figs. 3–5 (and from Fig. 6 in the next section) that the height of the first peak in diffuse transmittance is not strongly dependent on the period of the grating, after the transition from the subwavelength regime at low periods. The reason for this is that at the onset of each new grating mode, the interference is between the n_{00} mode, whose effective index only changes very slowly with the grating period, and a mode with $n^{eff}=n_g$. Thus the optimum height is the same at the onset of each grating mode. Between the onset of the grating modes the optimum height rises slowly as n^{eff} increases until the onset of the next grating mode.

C. AlGaAs pillars on GaAs

We can also use the method described here to understand optimum values of systems outside the range of strict applicability of the EIM and simplified modal analysis. The most comprehensive experimental investigation of light trapping and extraction with pillar grating structures used AlGaAs/GaAs quasiperiodic gratings formed by nanosphere lithography to increase the efficiency of light-emitting diodes[3] (and also to increase the photogenerated current when they were operated as solar cells). In this section we compare the results of simplified modal analysis using the EIM with the results of RCWA and with these experimental results.

Figure 6 shows RCWA results for a circular pillar grating of AlGaAs on a GaAs substrate along with the peak heights of the diffuse transmittance as calculated with the EIM. The RCWA results for circular pillar gratings and square pillar gratings (not shown) are very similar, for the same values of L and f (where f is the fraction of area covered by the pillars). That is, for lamellar gratings the grating period and the fractional area covered by the pillars are the

main factors determining the optimum grating structure, and the shape of the pillars is much less important. Thus the EIM gives good agreement with the RCWA results, even though the EIM results were calculated for a square pillar grating.

The results of the experimental optimization for this structure showed that photoluminescence (PL), light extraction, and photogenerated current increased sharply as pillar height increased up to 180 nm, with a further very slow increase up to a height of 350 nm (the maximum height studied). This behavior was similar for pillar diameters of 300 and 700 nm. From the results of RCWA in Fig. 6 we can see that there is a similar dependence on height for all values of L. As in the experimental results, there is a steep increase in diffuse transmittance up to a height of 150–200 nm (depending on grating period), followed by a slower increase, up to a height of around 300 nm or more. Figure 6 also shows that for a fixed height of 180 nm, there is a peak in the diffuse transmittance at around $L=400$ nm, which corresponds to a pillar diameter of 320 nm, in very good agreement with the experimentally determined optimum pillar diameter of 300 nm for a pillar height of 180 nm. Both the experimental results and the RCWA results show a decrease in diffuse transmittance as the period is increased to 500 nm (corresponding to a pillar diameter of 400 nm). In the period range of 500–900 nm (pillar diameter of 400–720 nm) the RCWA results show a slight increase while the experimental results show a slight decrease. Overall we can see that the results of RCWA and the EIM fit very well with experimentally determined values for this system, even though the experimental results were measured for a structure that was only quasiperiodic, formed by nanosphere lithography. Thus simplified modal analysis with the EIM is a useful tool for identifying the modes taking part and predicting the optimum grating heights even for diffractive structures that are only quasiperiodic, and even for structures where the pillars are circular rather than square.

D. Gratings and quantum dot superlattices

It is interesting to note that the 1D grating or photonic crystal equation [Eq. (2)] has exactly the same form as the equation for the 1D band structure of a superlattice of quantum wells in the case where the energy is above the barrier:

$$\cos(k_x^W L_W)\cos(k_x^B L_B) - \frac{1}{2}\left(\frac{k_x^B m_W^*}{k_x^W m_B^*}\right.$$
$$\left. + \frac{k_x^W m_B^*}{k_x^B m_W^*}\right)\sin(k_x^W L_W)\sin(k_x^B L_B) = \cos(k_x L). \quad (15)$$

Here L_W is the width of the well region, L_B is the width of the barrier region, and m_W^* and m_B^* are the effective masses in the well and barrier regions, respectively. The profile of the potential V for a superlattice is similar to the plan view of the profile for the corresponding grating, with $V=0$ in the well regions (corresponding to the ridges of the grating), and $V =V_0$ in the barrier regions (corresponding to the grooves of the grating).

The reason that the characteristic equations have the same form is that the form in each case is determined from only the following information: (i) the Schrödinger equation and Maxwell's equations are wave equations, with solutions that have a sinusoidal form for these boundary conditions; (ii) the solutions and their derivatives are continuous at the boundaries, and (iii) the boundary conditions are periodic. In quantum dot superlattices separate "resonant quasidiscrete" energy levels appear above the barrier for large interdot distances,[23] and we can see from the above discussion that these are directly analogous to the grating modes discussed here (also known as Bloch modes in the context of photonic crystals).

For the case of a superlattice in 2D or three dimensional (3D), the profile of the potential V is immediately approximately separable because the potential has an arbitrary additive constant, and hence the potential in the well region can be set to zero. This means that the structure can be described by Eq. (15) in each of the dimensions in which periodicity occurs,[23] and the allowed values of $k_x^{W,B}$ are the same as in the 1D case. For the grating or photonic crystal, there is no arbitrary additive constant and we must apply the EIM to find an approximately separable profile. Because the approximately separable profile of the grating has a lower dielectric function contrast than the original profile, the values of $k_z=k_0 n^{\text{eff}}$ are smaller in the 2D case than in the 1D case and [from Eq. (3)] the k_x values are larger.

IV. CONCLUSIONS

In this paper we have shown that grating mode interference provides a physically intuitive model of the behavior of square pillar gratings as a function of grating height and period, and incident wavelength. Pillar-type gratings offer a substantial performance benefit over groove-type gratings and are also potentially easier to fabricate. The effective refractive indices of the grating modes can be calculated approximately using the effective index method, which allows us to predict the optimum grating height and an estimate of the optimum period for gratings, without the need for extensive numerical calculations. Furthermore, the method also gives good results for structures outside the range for which it was derived, including circular pillars and quasiperiodic structures. We also point out the parallels between pillar diffraction gratings and the above gap states of quantum dot superlattices.

ACKNOWLEDGMENTS

[1] R. H. Morf, H. Kiess, and C. Heine, in *Diffractive Optics for Industrial and Commercial Applications*, edited by J. Turunen and F. Wyrowski (Akademie, Berlin, 1997), p. 361.
[2] A. A. Abouelsaood, S. A. El-Naggar, and M. Y. Ghannam, Prog. Photovoltaics **10**, 513 (2002).
[3] R. Windisch *et al.*, IEEE Trans. Electron Devices **47**, 1492 (2000).
[4] A. V. Tishchenko, Opt. Quantum Electron. **37**, 309 (2005).
[5] T. Clausnitzer, T. Kampfe, E. B. Kley, A. Tunnermann, U. Peschel, A. V. Tishchenko, and O. Parriaux, Opt. Express **13**, 10448 (2005).
[6] K. R. Catchpole, J. Appl. Phys. (to be published).

[7]K. S. Chiang, IEEE Trans. Microwave Theory Tech. **44**, 692 (1996).

[8]K. S. Chiang, Appl. Opt. **25**, 348 (1986).

[9]S. Mishra and S. Satpathy, Phys. Rev. B **68** (2003).

[10]P. Lalanne, J. P. Hugonin, and P. Chavel, J. Lightwave Technol. **24**, 2442 (2006).

[11]S. H. Fan and J. D. Joannopoulos, Phys. Rev. B **65** (2002).

[12]J. M. Pottage, E. Silvestre, and P. S. Russell, J. Opt. Soc. Am. A Opt. Image Sci. Vis **18**, 442 (2001).

[13]R. M. Knox and P. P. Toulios, in *Proceedings, Symposium on Submillimeter Waves*, edited by J. Fox (Polytechnic, Brooklyn, NY, 1970), p. 497.

[14]K. S. Chiang, Opt. Quantum Electron. **26**, S113 (1994).

[15]G. Lifante, Phys. Scr., T **T118**, 72 (2005).

[16]K. S. Chiang, J. Lightwave Technol. **5**, 737 (1987).

[17]E. A. J. Marcatili, Bell Syst. Tech. J. **48**, 2071 (1969).

[18]M. G. Moharam and T. K. Gaylord, J. Opt. Soc. Am. **72**, 1385 (1982).

[19]M. G. Moharam, E. B. Grann, D. A. Pommet, and T. K. Gaylord, J. Opt. Soc. Am. A Opt. Image Sci. Vis **12**, 1068 (1995).

[20]Gsolver (Grating Solver Development Company).

[21]A. Kumar, D. F. Clark, and B. Culshaw, Opt. Lett. **13**, 1129 (1988).

[22]K. S. Chiang, Opt. Lett. **16**, 714 (1991).

[23]O. L. Lazarenkova and A. A. Balandin, J. Appl. Phys. **89**, 5509 (2001).